Integrated Testing of Iodine BIT-3 RF Ion Propulsion System for 6U CubeSat Applications

IEPC-2017-264

Presented at the 35th International Electric Propulsion Conference
Georgia Institute of Technology • Atlanta, Georgia • USA
October 8 – 12, 2017

Michael Tsay[1], Joshua Model[2], Carl Barcroft[3], John Frongillo[4], Jurg Zwahlen[5], Charlie Feng[6]
Busek, Co. Inc., Natick, MA, 01760, U.S.A.

Abstract: Busek is developing an iodine-fueled RF ion propulsion system that will fly on two 6U CubeSats missions as part of NASA's upcoming SLS EM-1 launch in 2019. The 70W-nominal propulsion system utilizes a 2.5cm-grid-diameter RF ion thruster "BIT-3" and a micro RF cathode "BRFC-1" as the neutralizer. Other notable subsystem components include a custom thruster gimbal capable of 2-axis, ±10^{o} actuation, a lightweight tank designed for 87% propellant fraction, and a State-of-the-Art miniature Power Processing Unit (PPU) with >84% overall efficiency. The 1.5kg-dry/3.0kg-wet system, self-contained within an ultra lightweight aluminum chassis, is expected to produce 0.66-1.24mN thrust and 1,400-2,640sec Isp, at 56-80W throttleable PPU input power. When given sufficient power to operate, it can provide up to 37kN-sec total impulse and 2.9km/s deltaV for a 6U/14kg CubeSat. This paper details various subsystem- and system-level integrated testing results to date, including integrated mechanical system hot fire and gimbal-chassis random vibration test. The second part of the paper focuses on the development and testing of the flight PPU subsystem, including a demonstration of thruster-cathode hot fire with the full suite of PPU breadboards. Within the PPU subsystem, further details are presented regarding the innovative, dual-channel RF amplifier that has recorded a class-leading 90% DC-to-RF power conversion efficiency.

I. Introduction

The trend of the small satellite market in recent years has shifted towards the MicroSat class (10-100kg), with increased popularity among 6U and 12U CubeSats. As new technologies are developed and existing technologies become smaller and more power-efficient, these CubeSats are being used or proposed for new and incredible missions in and beyond Earth orbit. Commercially speaking, 6-12U CubeSats are very attractive as they represent a perfect balance between low development/launch cost and sufficient capability. When used in constellation configurations, they are well suited for the burgeoning remote sensing market. Although most of the larger CubeSats to date do not have onboard propulsion, the industry is not averse on the concept should propulsion system risks become manageable. After all, even a modest propulsive capability can help CubeSats stay in orbit longer (hence reducing fleet replenishment cost), maintain higher pointing accuracy, and conduct better science.

A few high-performance electric propulsion (EP) systems are currently available for CubeSats. They are in various stage of maturity. A survey of current State-of-the-Art (SOTA) options can be found in Ref. 1 and 2. One of these options that will soon reach Technology Readiness Level (TRL) 6 is Busek's iodine-fueled, "BIT-3" radio-

[1] Director, Electrothermal Propulsion Group, mtsay@busek.com
[2] Senior Electrical Engineer, Electronics Group, jmodel@busek.com
[3] Electrical Engineer, Electronics Group, cbarcroft@busek.com
[4] Mechanical Engineer, Electrothermal Propulsion Group, jfrongillo@busek.com
[5] Senior Engineer, Electrothermal Propulsion Group, jurg@busek.com
[6] Mechanical Engineer, Electrothermal Propulsion Group, cfeng@busek.com

frequency (RF) ion propulsion system.[3] Busek is scheduled to deliver flight BIT-3 systems by Q1 CY2018 to two 6U CubeSat missions manifested on NASA's SLS EM-1 launch: "Lunar IceCube" led by Morehead State University (shown in Figure 1) and "LunaH-Map" led by Arizona State University.[4,5] The two complementary science missions will be searching for water ice (Lunar IceCube) and hydrogen signatures (LunaH-Map) on the Moon's surface, and they will arrive at their final science orbit using the onboard BIT-3 ion propulsion.

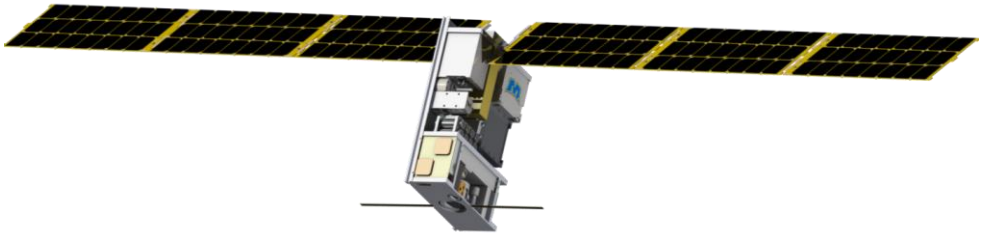

Figure 1. Lunar IceCube spacecraft model in flight configuration, showing BIT-3 system at the bottom of the spacecraft. Photo credit: Dr. Ben Malphrus, Morehead State University.

II. Background on Iodine BIT-3 Ion Propulsion System

Miniaturization of gridded ion thrusters (a.k.a ion engines) is a field that has seen some exciting progress in the recent years.[6,7,8] In 2015, Busek published the results of the first prototype BIT-3 RF ion thruster and its groundbreaking iodine propellant demonstration.[9] Further performance validations for the iodine BIT-3 thruster, and the combined operation with an iodine-compatible RF cathode neutralizer, were published recently.[10,11] The operation principle of RF ion thrusters is rather simple: an helical coil is energized at high frequency to create an inductive plasma, and positively charged ions are extracted and accelerated via grids to generate thrust. The electrostatic thrusting mechanism is identical to other types of gridded ion thrusters. RF ion thrusters, however, stands out among all EP devices because it has a unique characteristic of being inherently compatible with iodine propellant. This is because their plasma-containment chambers are exclusively made of corrosion-resistant ceramic materials (as iodine is a corrosive halogen). The ability to use iodine as propellant is a true game-changer for CubeSat propulsion, because iodine can be stored as a dense solid, and its sub-psi storage and operating vapor pressure is safe to launch while allowing for very lightweight and conformal tanks. In contrast, legacy EP propellant xenon has to be stored as highly compressed gas (>2,000psi) and requires bulky, spherical-shaped pressure vessels that are unfavorable for CubeSat's unique form factors. Pictured in Figure 2, Busek's BIT-3 RF ion thruster and its complementary BRFC-1 RF cathode neutralizer is the world's first EP thruster/cathode pair ever demonstrated with iodine propellant. This achievement is significant because the BIT-3 system, when augmented by iodine's unique packaging attributes, has significant total impulse advantages that can enable a very large class of CubeSat missions. Note that other benefits of using iodine as an EP propellant have been extensively covered by literatures (see Ref. 9, 12 and 13). Although iodine does not necessarily offer thrust or Isp advantages over xenon, it can still be considered as the better choice for CubeSat propulsion owing to its high storage density, near-zero vapor pressure (for launch safety), and minimum mass and volume requirements for the propellant tank.

Figure 2. Prototype BIT-3 RF ion thruster and BRFC-1 RF cathode neutralizer shown with xenon propellant (left), iodine propellant (middle), and flight configuration (right).

III. BIT-3 System Description

Figure 3 show the BIT-3 system configuration and its major subsystem components in Qualification Model (QM) maturity. Operational principle of the system can be found in Ref. 10 and 14. The BIT-3 system has a physical envelope of 180×88×102mm (~1.6U) and a 1.5kg dry mass. All components are mounted within a dip-brazed

aluminum chassis that weighs a mere 258g. In addition to the thruster and cathode, other notable subsystem components include a 2-axis thruster gimbal, a highly miniaturized Power Processing Unit (PPU), commercial-of-the-shelves (COTS) valves and pressure transducer, and a lightweight, rectangular-shaped propellant tank. The expected performance of the BIT-3 system is based on actual thrust and Isp data measured with iodine propellant[11] and bench-tested PPU efficiency, with some estimation on the system's on-orbit heater power requirement. The flight BIT-3 system will be throttleable between 56 and 80W at the PPU input. Expected thrust and Isp within this power range are 0.66-1.24mN and 1,400-2,640sec, respectively. The 80W max power is not outrageous for 6U CubeSats, as SOTA deployable solar array for 6U (as shown in Figure 1) can generate up to 120W prime power. When given sufficient power, the iodine BIT-3 system can provide total impulse up to 37kN-sec, giving a 6U/14kg CubeSat an unprecedented deltaV capability of 2.9km/s.

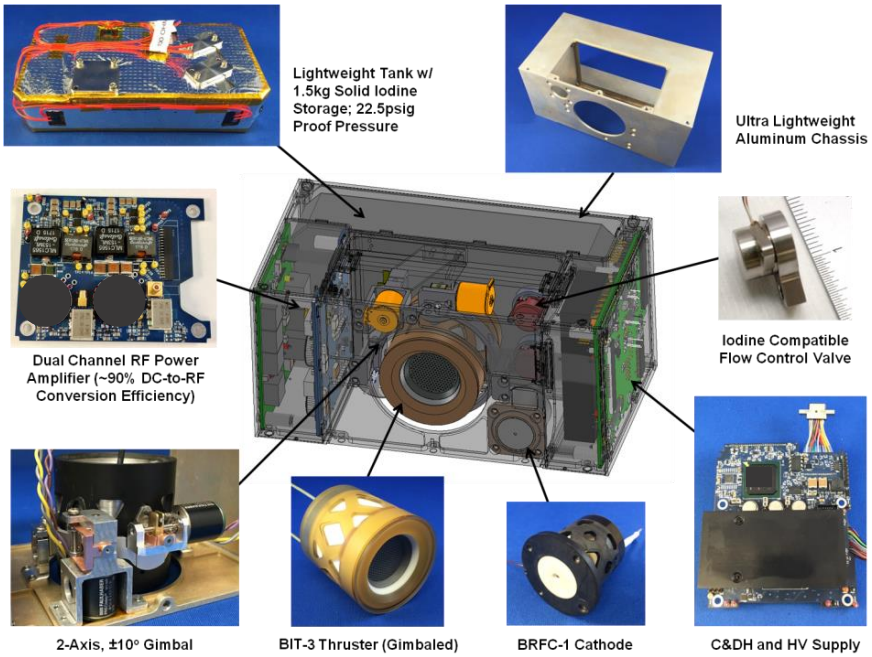

Figure 3. Major BIT-3 system components.

The all-metal propellant tank (Figure 4) weighs 208g dry and can hold up to 1.5kg of solid iodine, achieving a propellant mass fraction of 87%. Note that propellant filling is not a trivial task, as stock iodine comes in loose flake form with occupied density less than 2g/cc. In order to fill the tank to the designed mass fraction, which requires >4.3g/cc filling density, the iodine flakes must be liquefied and re-frozen inside the tank. This concept may sound simple, but execution can be extraordinarily difficult due to iodine's much increased corrosiveness in liquid state. A custom filling station was developed by Busek to mitigate such problem. Figure 4, right, shows the QM tank filled with 1.5kg iodine and integrated with patch heaters, multi-layer insulation (MLI), flight valves, and pressure transducer. This fully assembled propellant storage and feed system weighs approximately 1,880g wet.

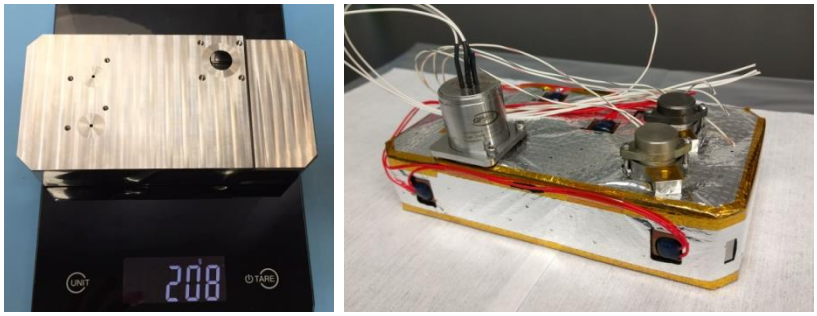

Figure 4. Iodine propellant tank: dry tank (left) and fully assembled QM feed system (right).

The BIT-3 gimbal utilizes two flight-grade stepper motors and is capable of ±10° rotation in <0.05° resolution. The gimbal enables a single primary thruster to de-saturate the Reaction Wheel Assembly (RWA) while in deep space. Three-axis attitude control with a two-axis gimbal can be challenging, but theoretically doable according to

Ref. 15. The concept calls for controlling the momentum directly on the Pitch and Yaw axes, but indirectly on the Roll axis via a spiral thrust maneuver. The gimbal can also help re-align thrust vector with spacecraft C.G., as C.G. may shift during flight due to propellant expenditure.

The BIT-3 gimbal operates on a linear actuation mechanism, which involves a pair of micro stepper motors each driving a lead screw. The linear actuator provides displacement in either (+ or -) direction on each axis. A custom limit switch is incorporated on each axis of travel. The limit switches are normally in the closed state (short circuit), which becomes open when the gimbal rotates to its designed extremity of $\pm 10^{o}$. Figure 5 shows the QM gimbal model and actual hardware as installed in the QM chassis.

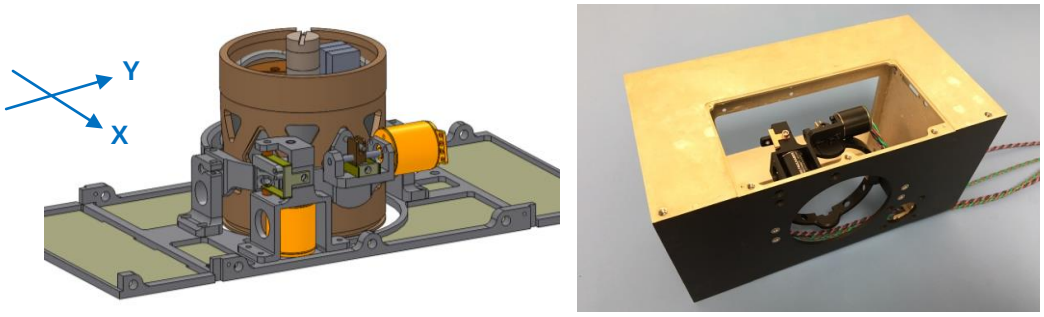

Figure 5. QM Gimbal CAD View (Left) and Assembled Hardware in Chassis (Right)

IV. Integrated Mechanical System Testing

QM Gimbal-Chassis Integrated Test

The QM gimbal assembly was extensively tested for functionality and rigidity along with the QM chassis. Functionality was verified with the use of a dummy thruster and a center-mounted laser, which helped determine motor step-to-angular rotation resolution and range limits by tracking laser illumination on a target plate. This setup is shown in Figure 6, with demonstration shown in Figure 7. The test successfully verified $\pm 10^{o}$, full range actuation along both axes, with rotational resolution of 0.04° per motor step in the X-axis, and 0.043° per step in the Y-axis. Note that in Figure 7 the gimbal and chassis were installed in a fixture prior to random vibration tests.

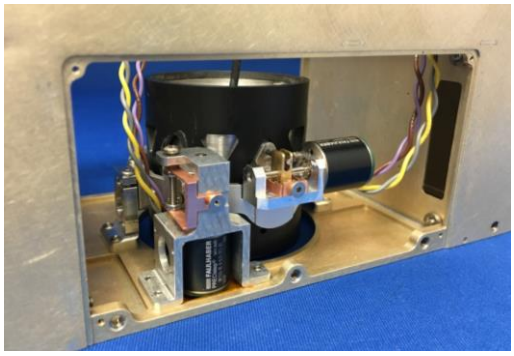

Figure 6. QM gimbal with dummy thruster and center-mounted laser, as seen in QM chassis.

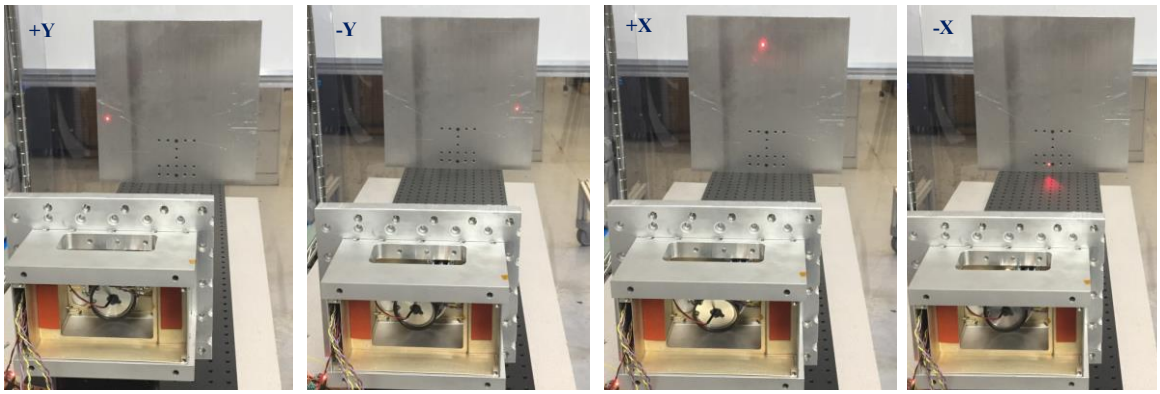

Figure 7. Demonstration of QM gimbal actuation and resolution with center-mounted laser.

The integrated QM gimbal and chassis were tested for random vibration, to levels published by NASA's General Environmental Verification Standard (GEVS). The vibe-test configuration, shown in Figure 8, consisted of the QM gimbal with integrated laser (for displacement testing before and after vibe) and a 1.7kg dummy tank mass with MLI over-wrap, both installed in a QM chassis. This test setup was installed in the BIT-3 system vibe fixture, which simulates the mechanical interfaces among BIT-3, host spacecraft, and launch deployer. The fixture included attachments of a control accelerometer hard mounted to the baseplate, and three tri-axial response accelerometers for monitoring the gimbal's frequency responses.

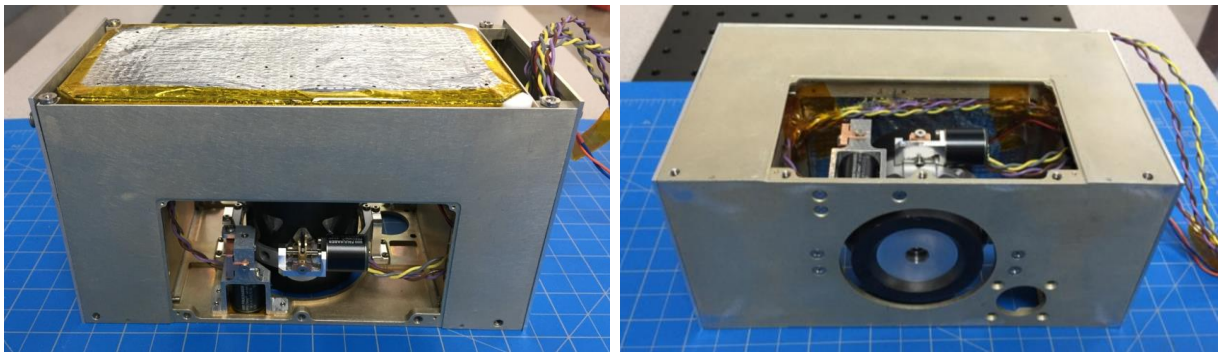

Figure 8. QM gimbal, chassis and dummy tank mass configured for random vibration test.

The QM gimbal-chassis setup went through two separate random vibration tests, first to GEVS Acceptance level and then to GEVS Qualification level. The test profiles are replicated in Figure 9. During the Qual level vibe, the Z axis was significantly over-tested to 20G composite, while the X and Y axis adhered to the GEVS Qual guideline of 14.1G composite. Such over-test was our way to reduce risks and further prove the gimbal for other potential launch platforms. In addition to verify gimbal's functionality post-vibe, we were also looking for confirmations that the hardware's natural frequency was sufficiently high (indicating a stiff structure), and there was minimum shift in the resonant frequency. The results were indeed satisfactory, in that:

- There was no natural resonance frequency less than 300Hz for the gimbal, and all natural frequencies were within 10% of each other between the two vibe tests (indicating response repeatability in the design, and system strength sufficient for the higher GEVS environment).
- All frequency shifts between pre- and post-vibe were within 20% and accompanied by almost no increase in amplification, indicating the units survived the qualification level loads with no decrease in capability.
- The gimbal showed no free movement during the test.
- A post vibe functional test was performed, and the results were nearly identical to the ones from the pre-vibe range limit and step resolution test.

Frequency	ASD Level, g^2/Hz (60sec per Axis)	
Hz	Qualification	Acceptance
20	0.026	0.013
20 – 50	+6 dB/oct	+6 dB/oct
50 – 800	0.16	0.08
800 – 2000	-6 dB/oct	-6 dB/oct
2000	0.026	0.013
Composite	14.1 G-rms	10.0 G-rms

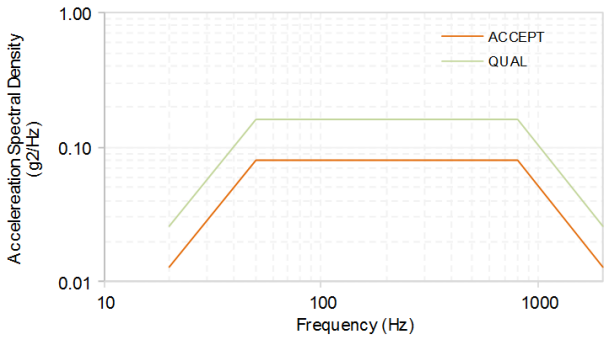

Figure 9. Random vibe levels tested with the QM gimbal and chassis.

Integrated Mechanical System Test

The integrated mechanicam system, including thruster, cathode, gimbal, chassis and feed system, was tested. The tests were first performed with xenon and then with iodine propellant. The primary objective of the initial xenon test was to verify hardware functionality in a tightly integrated setup. Specifically, the question of how the gimbal would operate next to the thruster and cathode's RF field, and how the system as a whole would perform temperature-wise were answered. The test setup, shown in Figure 10, consisted of Engineering Model (EM) thruster and cathode, and

QM gimbal and chassis. An EM iodine feed system was integrated into the chassis for the follow-on iodine test. The EM iodine feed system was similar to the QM unit shown previously in Figure 4, except for the use of larger (and less expensive) COTS solenoid valves rather than flight valves.

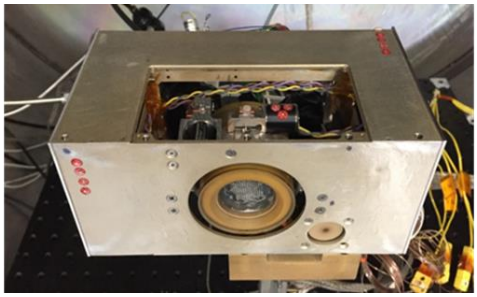

Figure 10. Integrated BIT-3 mechanical system (thruster-cathode-gimbal-chassis) test setup.

The xenon test sequence is summarized below, with test images captured in Figure 11 and Figure 12:

- The cathode's RF plasma was first ignited with an electric starter, which initiated a pilot glow discharge upstream of gas inlet and supplied seed electrons to the cathode's discharge chamber (Figure 11 a).
- After the cathode was on, its internal ion collector electrode was biased to the "Boost" mode of -100V. Electrons were actively ejected toward a virtual anode (ground) outside of the cathode's exit (Figure 11 b).
- With plenty free electrons in the ambient, the thruster's plasma was ignited by switching the polarity of its downstream Accelerator grid and drawing in seed electrons from the cathode (Figure 11 c).
- Once the thruster's plasma was ignited and the ion beam was formed, the cathode's electron emission mechanism was switched to a power-saving passive mode, via a phenomenon known as "plasma bridge".[11,16] This allowed the cathode's ion collector voltage to reduce to its "Normal" setting of -10V. The ion beam then drew out matching electron current from the cathode for neutralization (Figure 11 d).
- After the thruster and cathode reach steady-state operation, the gimbal was commanded to move to its 10-degree extremities (Figure 12).

The test was successful on all accounts, with the gimbal operating through its full range of motion during thruster and cathode firing, no signs of startup inhibitng or neutralization prevention due to chassis interference, minimal performance loss of the thruster and cathode due to RF-chassis & RF-gimbal ring interactions, and successful temperature mapping of chassis temperature rise during the period of operation.

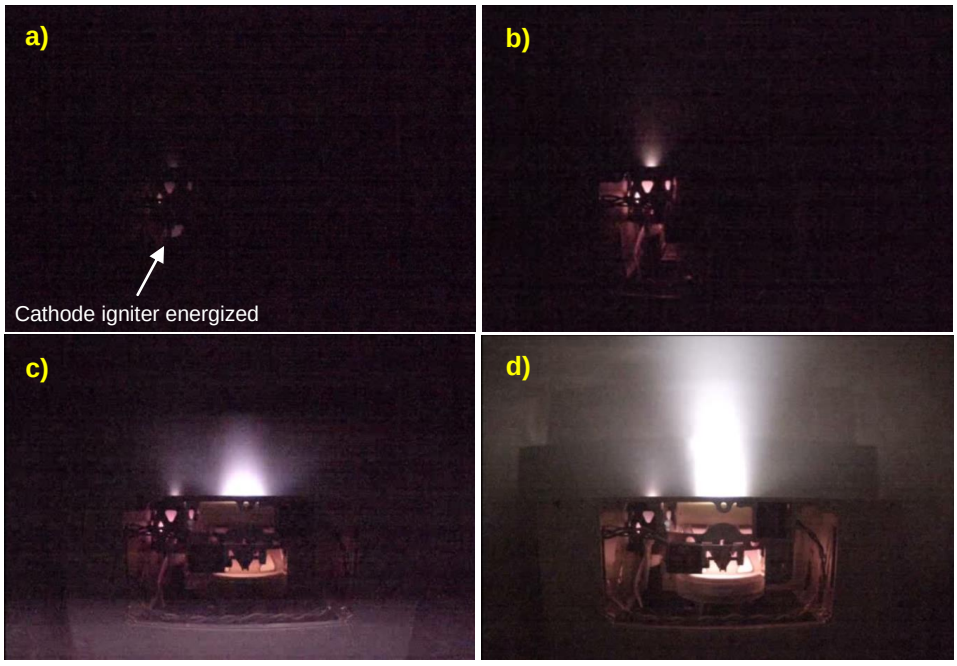

Figure 11. BIT-3 system startup, shown with xenon propellant: a) cathode ignition, b) cathode in Boost mode, c) thruster ignition by drawing in cathode emission, d) steady-state thruster and cathode operation.

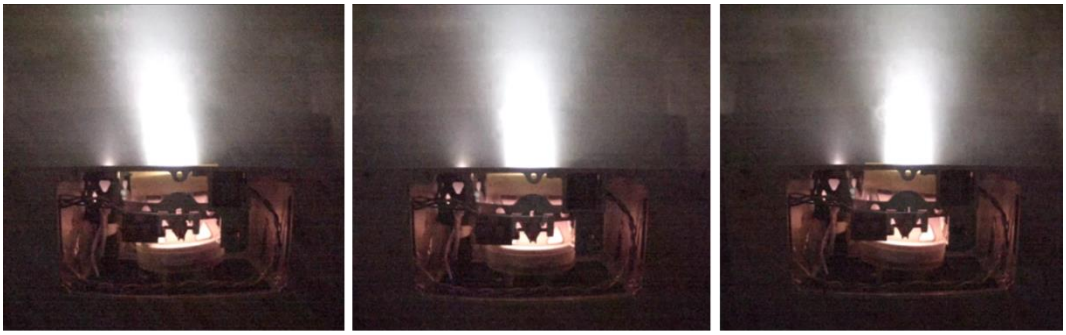

Figure 12. Gimbal operation during hot firing (xenon shown).

After the successful xenon test, the EM iodine feed system was installed in the chassis. The system-level iodine hot-fire test is currently ongoing, but results to date have shown similar startup conditions as compared to the xenon test. Figure 13 shows the different looks of the RF cathode during steady-state operation, with the two different propellants. Upon completion of the current iodine test, the thruster, cathode and feed system will be replaced by QM units, followed by integration of the QM PPU and harness.

Figure 13. BRFC-1 RF cathode operating on xenon (left) and iodine (right) propellant.

V. PPU Development and Testing

BIT-3's PPU handles spacecraft to propulsion system interfacing, by converting bus power and commands to formats usable within the BIT-3 system. The PPU's design methodology balances competing requirements for radiation tolerance, low cost, low mass and tight design volume. Figure 14, left, shows the solid model of the BIT-3 flight system, highlighting the unique split PPU design and wire harness. The two halves of the PPU are connected via a 31-pin Nano-D connector and a flexible cable assembly. The right PPU compartment houses the Command and Data Handling (C&DH) board, which contains a FPGA-based Digital Control Interface Unit (DCIU) that provides the monitoring and control functions to all BIT-3 system elements, as well as interfacing to the host vehicle. The C&DH board has a secondary function which is powering all low-voltage hardware in the system, including heaters, gimbal motors, propellant control valves, pressure transducer, and temperature sensors. It also integrates a COTS, 2kV converter module within its allocated volume, eliminating the need for an additional PCB for the thruster screen grid supply. The left PPU compartment houses the RF Amplifier board and the auxiliary High Voltage (HV Aux) board. The RF Amplifier board features a dual-channel, ~90% efficienct RF amplifier circuitry that powers the inductive plasma discharges in the thruster and cathode. The HV Aux board supplies the bipolar accelerator grid voltage for the thruster, the ion collector bias voltage for the cathode, and the transient high voltage required for the cathode igniter. Figure 14, right, shows the actual QM PPU hardware. The QM PPU has been loaded with flight-level software and bench-tested, and all communication interfaces (including external RS-485) have been verified. The complete PPU assembly, including cable harness, weighs less than 420g.

The BIT-3 PPU was designed for deep-space radiation environments where Single Event Upset (SEU) is more likely to occur than damages caused by excessive Total Ionizing Dose (TID). This is due to the fact that, for missions to GEO and beyond, the high-energy electron and proton environment is relatively benign, and the 0.100" aluminum skin of the spacecraft provides sufficient shielding to reduce the TID to low levels. However, heavier species are more plentiful and interactions with them can result in SEU. In particular, power electronics are susceptible to Single Event Burnout and Single Event Gate Rupture. The PPU design, however, cannot solely focus

on safeguarding against SEU because extensive use of screened, rad-hard components would make the boards too large and too costly to fabricate. Hence, the certain volume, performance and development costs of moving to specialty components must be weighed against the risk of a potential failure due to radiation effects. A balanced methodology was developed to evaluate and mitigate risk on a per mission basis, providing the best combination of cost, performance and mission assurance. The design follows a "Rad-Hard Fence" approach that provides the most assurance where a failure could cascade to peripheral functions.[10] For example, the BIT-3 PPU's C&DH and Housekeeping subassemblies follow conservative design approaches, with additional implementation of Triple Modular Redundancy on the rad-hard FPGA. Extra care was taken here because a failure in the PPU core could cascade to the entire system. Alternatively, the designs for the RF amplifier and the HV beam supply are allowed to be more aggressive in pursuit of performance. For these peripheral subassemblies, attention was still paid with regards to parts selection and radiation, for example by following the de-rating guide of EEE-INST-002, but the acceptable risk level is generally higher.

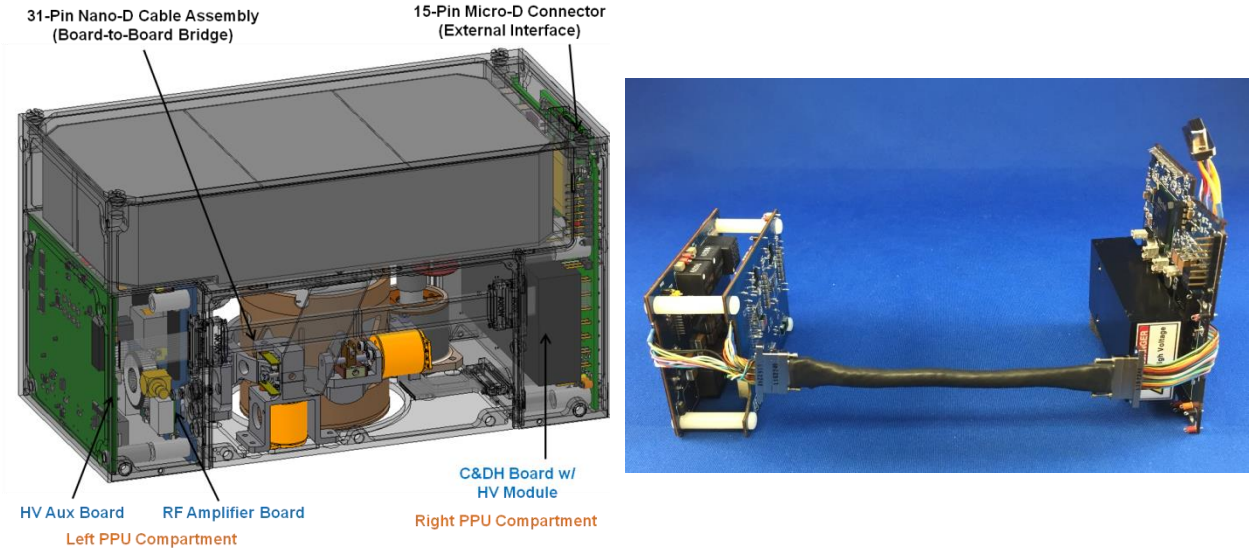

Figure 14. BIT-3 system's unique split PPU design (left) and QM PPU hardware (right).

RF Amplifier Board

The RF amplifier board is perhaps the most innovative component of the BIT-3 PPU. The initial design of the RF amplifier targeted minimum form factor and maximum DC-to-RF power conversion efficiency for operating the BIT-3 thruster and the BRFC-1 RF cathode. Since the two devices operate at different frequencies, initial breadboards for the RF amplifier were two discrete boards. They were later combined into a single PCB during QM development (Figure 15). The design methodology for the amplifiers consisted of a DC/DC converter outputting to a custom amplifier, with a power measurement circuit on the output waveform (Figure 16). Via an Analog-to-Digital Converter (ADC), the forward and reflect RF power measurements are fed back to the signal generator at the FPGA. The closed-loop control enables automatic independence matching by adjusting the driver frequencies on the fly. The driver frequency is synthesized digitally on the FPGA, without requiring additional resonator components.

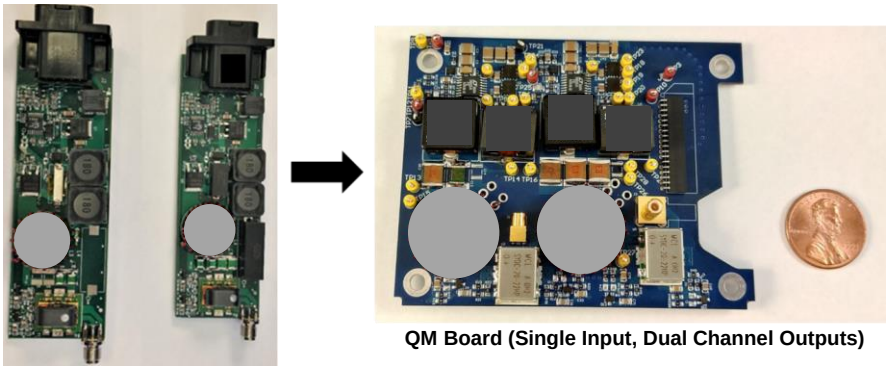

Figure 15. Evolution of RF Amplifier board.

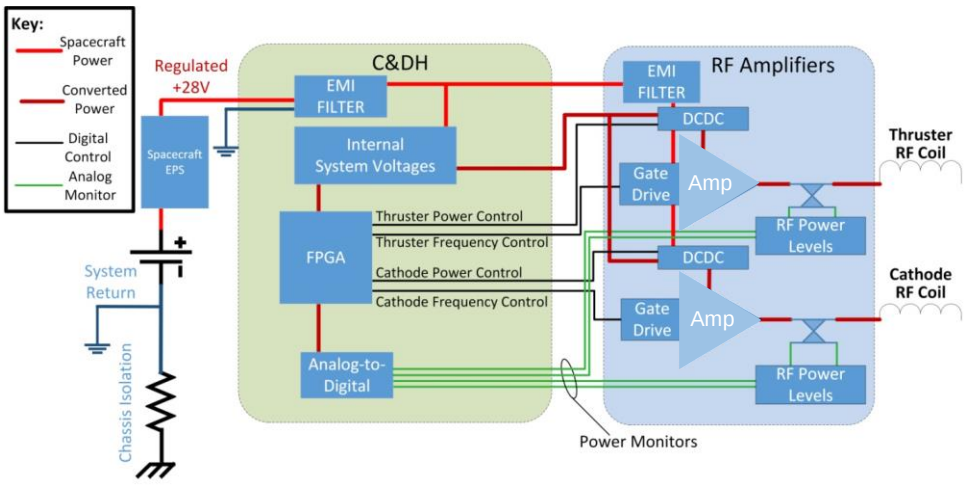

Figure 16. Block diagram of BIT-3 RF Amplifier design.

Bench testing of the QM RF Amplifier board confirmed an end-to-end, DC-to-RF power conversion efficiency of ~90% across a wide range of output level (Figure 17). To achieve such an extremely high efficiency, the RF board leverages a wide-bandgap semiconductor device in the switching circuitry. These devices can reduce switching losses to near negligible levels and maintain low conduction losses in the on-state. They are also known to be highly resistant to radiative TID. What's more, the voltage breakdown properties of the devices allow for extreme de-rating for our application, providing robustness against SEUs.

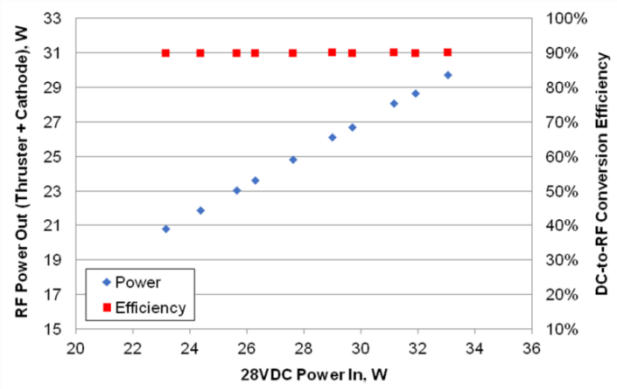

Figure 17. End-to-end test data of QM RF amplifier board.

RF Frequency Synthesizer Design

A finely-tunable frequency source is required to operate the RF amplifier board. Given the limited power and board space available, a solution contained solely within the C&DH board's FPGA was developed. The technique takes advantage of the FPGA's capability of operating small bits of logic at high speed, and the on-chip clocking resources available. The implementation results are shown in Figure 18. Some remaining jitter is evident, but this is reflective of peak-to-peak, not RMS jitter since the scope had infinite persistence enabled. Though at the limits of the scope's accuracy, this result indicates that the RMS jitter is less than 400ps, which is more than adequate for matching both the RF thruster and cathode's frequencies.

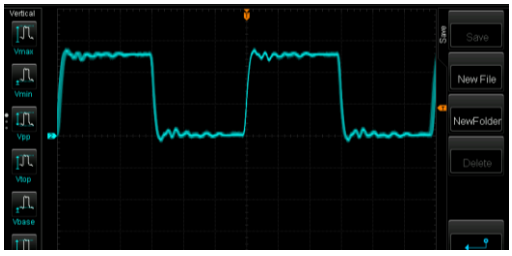

Figure 18. Direct digital synthesis of frequency waveform for driving RF amplifiers.

HV Aux Board

After breadboard verification, the QM HV Aux board was developed and tested, see Figure 19 and Figure 20. The board's cathode bias voltage output was demonstrated for both the normal bias voltage of -10V (for passive neutralization) and the "Boost" mode of -100V used during thruster ignition. The thruster Accel grid supply was also demonstrated, via switching between normal -200V supply and +200V supply during thruster ignition mode. Finally, the arc protection circuit of the Accel grid supply was tested, showcasing the circuit's ability to protect against arcs from the Screen grid during thruster operation, see Figure 21. The transient high-voltage supply for the cathode igniter was also tested successfully via actual cathode firing, though scope trace data were not available.

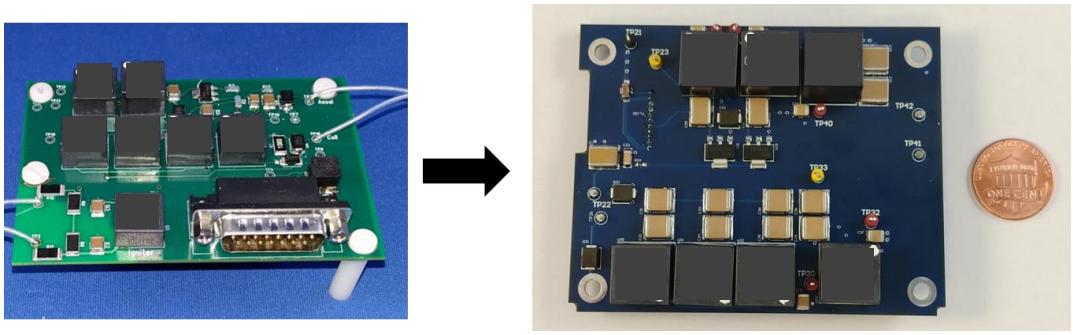

Figure 19. Breadboard HV Aux board (left) vs. QM HV Aux board (right).

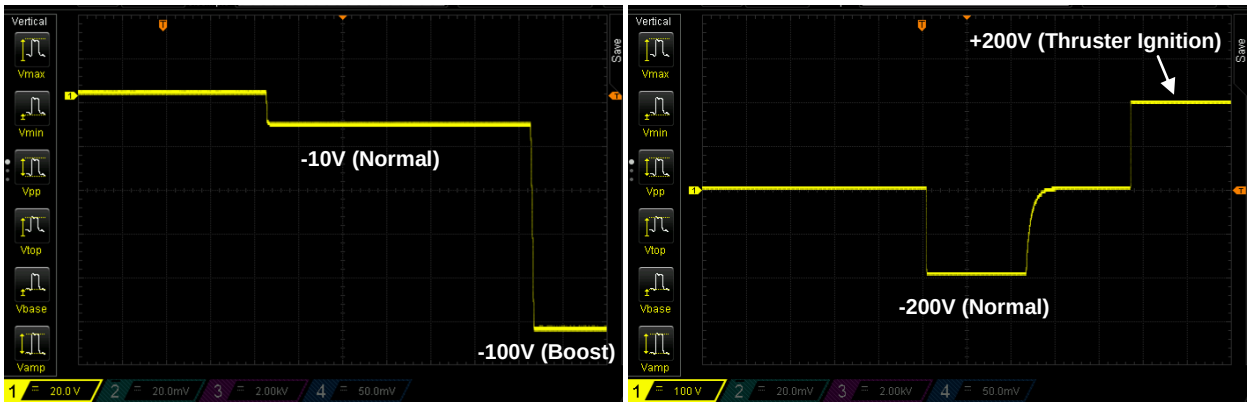

Figure 20. QM HV Aux board test results: cathode bias modes (left) and thruster Accel grid modes (right).

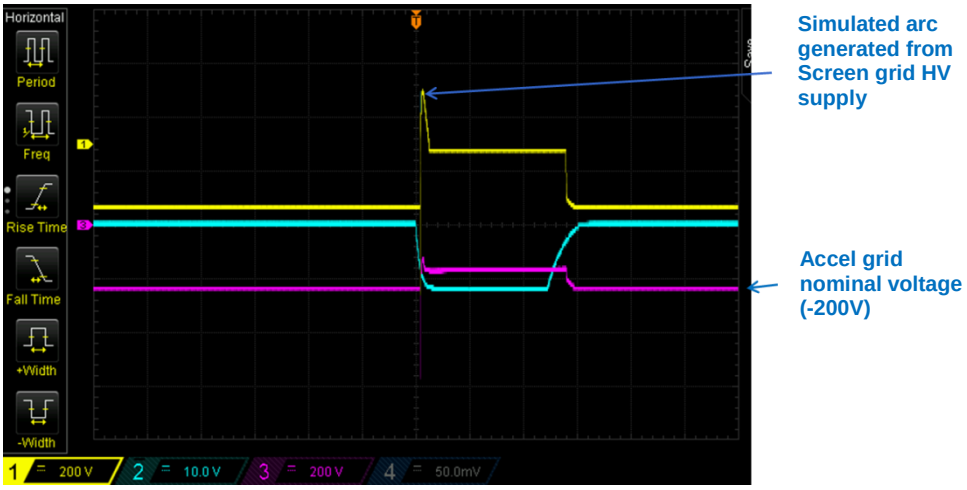

Figure 21. QM HV Aux board test result showing arc-protection on Accel grid supply.

C&DH Board

Due to strict PPU volume requirement, it was decided early on that the C&DH board and the 2kV converter for the thruster's Screen grid supply would be integrated into a single board, with the HV supply mounted on standoffs

to the PCB proper. A COTS HV supply module was selected and characterized via bench testing. The selected converter was first installed on a dedicated HV breadboard (without C&DH functions) and tested at temperature in a vacuum oven. Figure 22 shows the breadboard. The result ensured that the part exhibits no anomalies or behavior change under the expected temperature extreme. The HV supply demonstrated a nominal DC-to-DC power conversion efficiency of 84%. After breadboard verification, the HV supply module was integrated into the QM C&DH board, as shown in Figure 23 for both CAD model and actual hardware.

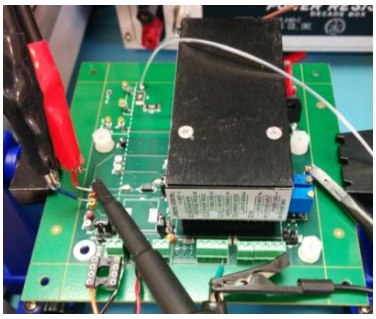

Figure 22. Screen grid HV supply module mounted on breadboard.

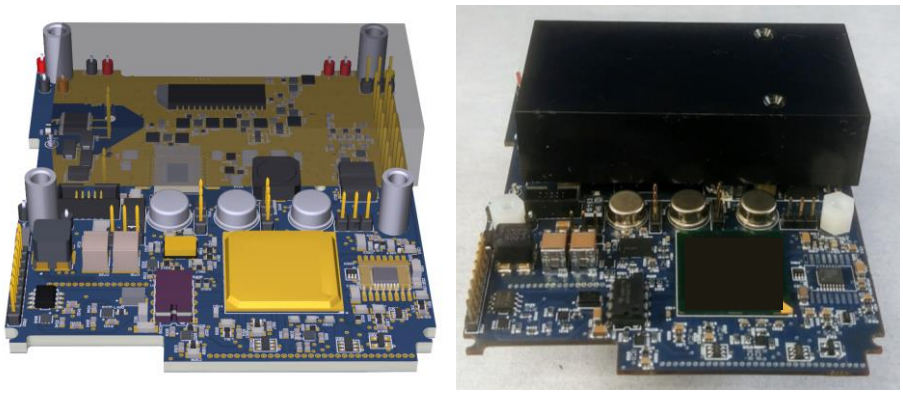

Figure 23. QM C&DH board with integrated HV supply module.

Breadboard PPU Integrated Test

Prior to QM development, the full breadboard PPU was integrated with a test panel and demonstrated by driving the hot fire of both the BIT-3 thruster and BRFC-1 cathode. This setup is shown in Figure 24. The test panel is a simulated C&DH fixture that offers direct, low-level control input. Full operation of the thruster and cathode were successfully carried out entirely from the test panel. This included cathode ignition, cathode emission boost, thruster ignition (Accel grid polarity switch) and thruster operation at nominal grid voltages. Both thruster and cathode discharges were powered by the RF amplifier breadboards. The DC-to-RF conversion efficiencies of these RF breadboards were verified to be ~90% with live plasma loads. These test results were an important milestone before production began on the tightly integrated QM PPU hardware, shown previously in Figure 14.

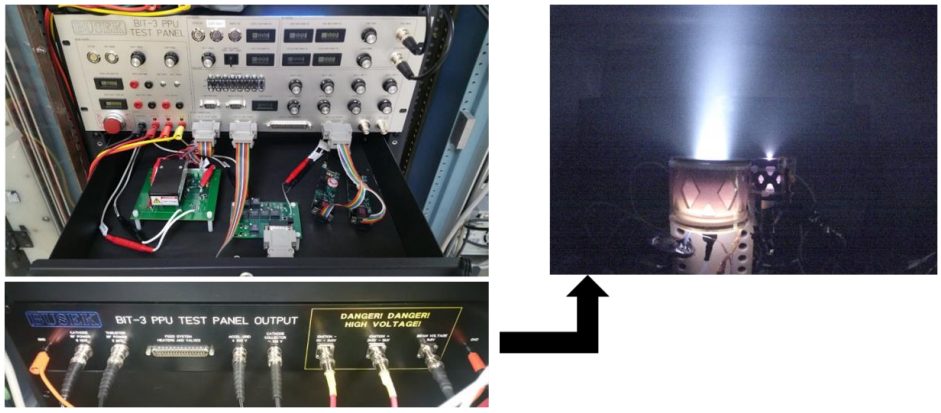

Figure 24. Full suite of breadboard PPU integrated with test panel, driving thruster and cathode hot fire.

VI. Conclusion

The most up-to-date hardware status of Busek's iodine BIT-3 ion propulsion system is given. All QM component was fabricated and tested following an extensive hardware development phase (EM results were previously reported in literatures). Various integration tests have been performed on both subsystem and system levels. The QM gimbal and chassis passed GEVS Qual random vibration test before undergoing integrated mechanical test with thruster, cathode and feed system. The integrated mechanical system hot fire was extremely successful with xenon propellant. The same setup is currently configured for iodine testing, and results have shown similar startup and operating conditions. Upon conclusion of the iodine test, the QM PPU will be integrated into the chassis for a final system demonstration, which will be followed by a full environmental qualification test.

Design and development of the BIT-3 PPU is also presented. The PPU employs an innovative RF amplifier that achieves a class-leading, ~90% DC-to-RF power conversion efficiency. Additional features of the RF amplifier include automatic impedance matching and on-chip frequency synthesis, both unique and State of the Art. The full suite of breadboard PPU was tested with live plasma loads via BIT-3 thruster and BRFC-1 cathode, before progressing to QM development. The QM PPU retains all breadboard functionalities but with extremely tight packaging. It weighs <420g including cable harness. The QM PPU achieves an overall efficiency of >84% with a regulated $28V_{DC}$ input.

Finally, based on all performance measurement results, a full iodine BIT-3 flight system is expected to produce 0.66-1.24mN thrust and 1,400-2,640sec Isp, at 56-80W throttleable PPU input power. The available 37kN-sec total impulse (at 80W) translates to a maximum of 2.9km/s deltaV for a 6U/14kg CubeSat. The system is on schedule for flight delivery to two SLS EM-1 CubeSats during Q1 CY2018.

Acknowledgments

The material for this publication is based upon the R&D work funded by NASA's Small Spacecraft Technology Program (SSTP) under the Space Technology Mission Directorate (STMD), managed by Dr. Wensheng Huang of NASA Glenn Research Center. The two deep-space CubeSat flight programs for the BIT-3 system are sponsored by NASA's Advanced Exploration Systems (AES) under the Human Exploration and Operations Mission Directorate (HEOMD) for Lunar IceCube, and Science Mission Directorate (SMD) for LunaH-Map. The authors would also like to thank Dr. Ben Malphrus of Morehead State University (principle investigator of Lunar IceCube) and Dr. Craig Hardgrove of Arizona State University (principle investigator of LunaH-Map) for their continuous support.

References

[1]Lev, Dan., et al., "The Technological and Commercial Expansion of Electric Propulsion in the Past 24 Years," 35th International Electric Propulsion Conference, Atlanta, GA, October 2017. IEPC-2017-242.

[2]Parker, K., "State-of-the-Art for Small Satellite Propulsion Systems," 2016 Biennial Aerospace Systems Conference of the National Society of Black Engineers (NSBE), Arlington, VA, August 2016, NASA Report no. GSFC-E-DAA-TN33641.

[3]Hargus, W., and Singleton, J., "Application of Technology Readiness Levels to Micro-Propulsion Systems," 52nd AIAA Joint Propulsion Conference, Salt Lake City, UT, July 2016, AIAA-2016-5113.

[4]Robinson, K., and Norris and G., "NASA's Space Launch System: Deep-Space Delivery for Smallsats," 31st AIAA/USU Conference on Small Satellites, North Logan, UT, August 2017, SSC17-IV-02.

[5]Tsay, M., et al., "LunarCube: A Deep Space 6U CubeSat with Mission Enabling Ion Propulsion Technology," 29th AIAA/USU Conference on Small Satellites, North Logan, UT, August 2015, SSC15-XI-1.

[6]Conversano, R. and Wirz, R., "CubeSat Lunar Mission Using a Miniature Ion Thruster," 47th AIAA Joint Propulsion Conference, San Diego, CA, August 2011, AIAA-2011-6083.

[7]Koizumi, H., et al., "In-Flight Operation of the Miniature Propulsion System installed on Small Space Probe: PROCYON," 34th International Electric Propulsion Conference, Kobe, Japan, July 2015, IEPC-2015-276/ISTS-2015-b-276.

[8]Leiter, H., et al., "Development of a Miniaturized RF Ion Engine System for Commercial and Scientific applications," 47th AIAA Joint Propulsion Conference, San Diego, CA, July 2011, AIAA-2011-6070.

[9]Tsay, M., et al., "Iodine Fueled Mini RF Ion Thruster for CubeSat Applications," 34th International Electric Propulsion Conference, Kobe, Japan, July 2015, IEPC-2015-273.

[10]Tsay, M., et al., "Maturation of Iodine Fueled BIT-3 RF Ion Thruster and RF Neutralizer," 52nd AIAA Joint Propulsion Conference, Salt Lake City, UT, July 2016, AIAA-2016-4544.

[11]Tsay, M., et al., "Neutralization Demo and Thrust Stand Measurement for BIT-3 RF Ion Thruster," 2017 AIAA Propulsion and Energy Forum, Atlanta, GA, July 2017, AIAA-2017-4890.

[12]Szabo, J, et al., "Performance Evaluation of an Iodine-Vapor Hall Thruster," *Journal of Propulsion and Power*, Vol. 28, No. 4, July-August 2012, pp. 848-857.

[13]Dankanich, J., et al., "Mission and System Advantages of Iodine Hall Thrusters," 50th AIAA Joint Propulsion Conference, Cleveland, OH, July 2014, AIAA-2015-3905.

[14]Tsay, M., et al., "Qualification Model Development of CubeSat RF Ion Propulsion System BIT-3,"31st International Symposium on Space Technology and Science, Matsuyama, Japan, June 2017, ISTS-2017-f-059.

[15]Randolph, T., et al., "Three-Axis Electric Propulsion Attitude Control System with a Dual-Axis Gimbaled Thruster," 47th AIAA Joint Propulsion Conference, San Diego, CA, August 2011, AIAA-2011-5586.

[16]Scholze, F., et al, "Performance Modeling of a Radio Frequency Plasma Bridge Neutralizer," Space Propulsion 2016 Conference, Rome, Italy, May 2016. SP2016_3124790.